Rigorous Modeling of the Kinetics of Calcium Carbonate Deposit Formation

Raviv Segev, David Hasson, and Raphael Semiat
Rabin Desalination Laboratory, Grand Water Research Institute, Dept. of Chemical Engineering, Technion–Israel Institute of Technology, Haifa 32000, Israel

DOI 10.1002/aic.12645
Published online April 27, 2011 in Wiley Online Library (wileyonlinelibrary.com).

The complexity of $CaCO_3$ deposit formation on a flow surface arises from the need to take into account the multicomponent transport of all ionic species involved in the carbonic system. Several semitheoretical and empirical models are available. This article presents a rigorous kinetic model that takes into account the diffusional transport of all species involved in $CaCO_3$ wall deposition under turbulent flow as well as the kinetics of the $CaCO_3$ crystallization reaction. Conditions under which high- and low-pH simplified expressions may be used are evaluated. It is shown that the simplified precipitation rate equations provide results within 10% of the rigorous solution when the high-pH expression is applied for solutions at pH levels above 9.5, and the low-pH expression is applied for solutions at pH levels below 7.6. © 2011 American Institute of Chemical Engineers *AIChE J*, 58: 1222–1229, 2012

Keywords: $CaCO_3$ precipitation kinetics, multicomponent ionic diffusion, scale deposition, simplified models, rigorous analysis

Introduction

The kinetics of $CaCO_3$ deposition on flow surfaces is of widespread interest in many engineering applications, notably cooling tower water systems and both thermal and membrane desalination processes. Comprehension of the kinetics of this system is closely allied to scale control efforts.

Numerous kinetic models had been proposed spanning from strictly empirical correlations[1–6] to expressions derived on the basis of physical and chemical considerations.[7–10] The kinetics of $CaCO_3$ precipitation continues to evoke conspicuous interest as evident from the steady publication of articles on this topic.[11–15]

The complexity of the $CaCO_3$ precipitation system arises from the need to consider the combined role of several mass transfer and chemical reaction processes. All available models are based on assumptions severely restricting their applicability. Approximate kinetic expressions for $CaCO_3$ carbonate deposition at low- and high-pH conditions developed by Hasson et al.[7,8] have been used in numerous studies.[9,11,14–16]

The aim of this article is to provide a rigorous kinetic analysis, which enables to assess the range of conditions at which the simplified equations are of sufficient accuracy. The system considered is wall deposition of a crystallizing $CaCO_3$ scale layer from a supersaturated solution in isothermal turbulent flow through a tube.

Precipitation Process

Balance equations

Figure 1 shows wall deposition of a crystallizing $CaCO_3$ layer from a supersaturated solution flowing through a tube. Bulk precipitation that may occur at high supersaturation conditions is neglected here. The overall reaction involved in the wall crystallization process of $CaCO_3$ is:

$$Ca^{+2} + 2HCO_3^- \rightarrow CaCO_{3(s)} + CO_2 + H_2O \qquad (1)$$

Correspondence concerning this article should be addressed to D. Hasson at hasson@technunix.technion.ac.il.

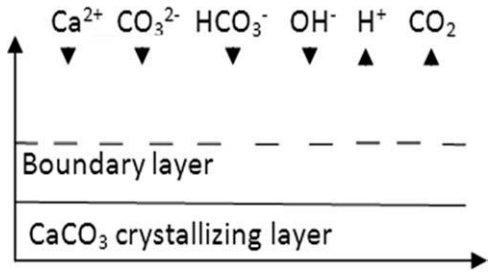

Figure 1. Transport of the reacting species from the solution bulk to the crystallizing layer.

The mechanisms involved are an initial crystallization reaction:

$$Ca^{+2} + CO_3^{-2} \rightarrow CaCO_{3(s)} \tag{2}$$

followed by shifts in the equilibria of the ionic species participating in the crystallization process:

$$H^+ + HCO_3^- \rightleftharpoons CO_2 + H_2O \tag{3}$$

$$HCO_3^- \rightleftharpoons H^+ + CO_3^{2-} \tag{4}$$

According to the above mechanism, reacting species (Ca^{2+}, CO_3^{2-}, HCO_3^-, and OH^-) are transported toward the deposition surface, and reaction products (H^+ and CO_2) are transported away from the surface. It is assumed that both the crystallization reaction (Eq. 2) and the carbonate reactions (Eqs. 3 and 4) are surface processes. The minor species involved in the above system ($CaOH^+$, $CaCO_3^0$, and $CaHCO_3^+$) are neglected here, because their influence is negligible under most practical scaling conditions.

The six species involved in the diffusional transport process accompanying the $CaCO_3$ crystallization process are Ca^{2+}, CO_3^{2-}, HCO_3^-, OH^-, H^+, and CO_2. An additional species involved in the interphase reaction is $CaCO_3$. A set of four independent reactions relating these species is as follows:

$$CO_2 + H_2O = HCO_3^- + H^+ \tag{5}$$

$$CO_2 + OH^- = HCO_3^- \tag{6}$$

$$HCO_3^- = H^+ + CO_3^{-2} \tag{7}$$

$$Ca^{+2} + CO_3^{-2} = CaCO_{3(s)} \tag{8}$$

With seven species and four independent reactions, three invariants of the system express mass and electrical balances interrelating the molar fluxes J_i of the various species:

$$J_{Ca^{+2}} \equiv J_{CaCO_3} \tag{9}$$

$$2J_{Ca^{+2}} = J_{HCO_3^-} + 2J_{CO_3^{-2}} + J_{OH^-} - J_{H^+} \equiv J_T \tag{10}$$

$$J_{Ca^{+2}} = J_{HCO_3^-} + J_{CO_3^{-2}} + J_{CO_2} \tag{11}$$

The physical significance of these balances is simple to interpret. Equation 9 states that the Ca^{2+} flux equals the crystallization rate. Equation 10 expresses conservation of electroneutratlity—the equivalent Ca^{2+} flux is balanced by the total alkalinity flux. Equation 11 states that the rate of $CaCO_3$ crystallization equals the rate of depletion of carbon species from the solution.

Diffusional transport equations

The general material balance of ionic species in a diffusional transport system is given by:

$$\frac{\partial c_i}{\partial t} + \nabla J_i = r_i \tag{12}$$

where c_i is the concentration of species i (mol/m^3), J_i is the ionic flux of species i (mol/m^{2}sec), and r_i is the rate of production of species i (mol/(m^3 s)). Diffusional transport of the ionic species is governed by the Nernst–Planck equation:

$$\mathbf{J}_i = -D_i\left(\nabla C_i + z_i C_i \frac{F}{RT}\nabla V\right) \tag{13}$$

where D_i is the diffusion coefficient of ion species i, C_i is its molar concentration, z_i is its charge, F is the Faraday constant, R is the universal gas constant, T is the temperature, and V is the electrical potential generated by the motion of ions having different diffusivities.

Combining Eqs. 12 and 13, the general material balance for species i is:

$$\frac{\partial c_i}{\partial t} + \nabla(-D_i\nabla c_i - z_i u_i F c_i \nabla V) = r_i \tag{14}$$

where u_i represents the mobility of species i (mol m^2)/(J s), and r_i is the rate of production of species i (mol/(m^3 s)). Solution electroneutrality is given by:

$$\sum z_i C_i = 0 \tag{15}$$

Also, as already verified by Eq. 10, the fluxes of the diffusing species conserve electroneutrality. In the absence of an electric current,

$$\sum J_i z_i = 0 \tag{16}$$

For a one-dimensional steady state system, Eq. 12 reduces to:

$$\frac{dJ_i}{dx} = r_i \tag{17}$$

and Eq. 13 simplifies into:

$$\mathbf{J}_i = -D_i\left(\frac{dC_i}{dx} + z_i C_i \frac{F}{RT}\cdot\frac{dV}{dx}\right) \tag{18}$$

Table 1 lists values of ionic diffusion coefficients at infinite dilution at 25°C.[17] It is seen that except for the hydrogen and hydroxyl ions, all other ions have closely similar diffusivities. For equal diffusivities, it can be readily shown

Table 1. Values of Ionic Diffusion Coefficient at 25°C at Infinite Dilution

D_H	$9.31\cdot\times 10^{-9}$ (m^2/s)	D_{HCO3}	$1.13\cdot\times 10^{-9}$ (m^2/s)
D_{OH}	$5.27\cdot\times 10^{-9}$ (m^2/s)	D_{CO3}	$0.97\cdot\times 10^{-9}$ (m^2/s)
D_{CO2}	$2.00\cdot\times 10^{-9}$ (m^2/s)	D_{Ca}	$0.79\cdot\times 10^{-9}$ (m^2/s)

that the electrostatic potential gradient $dV/dx = 0$ and ionic flux equations can be simply described by Fick's law.

In most cases, the neglect of the potential gradient term is justified even in the presence of the high diffusivities of the H^+ and OH^- ions for two reasons. The concentration levels of these ions are usually much smaller than those of the other ions, and also in mass transfer systems, diffusion is controlled by the slower moving ions.

Finally, it is of interest to note that the ionic strength level of the solution also acts to diminish the potential gradient term, as evident from the following expression derived from Eq. 18:

$$\frac{\mathrm{F}}{\mathrm{RT}}\cdot\frac{\mathrm{dV}}{\mathrm{dx}} = -\left\{\frac{\sum \mathrm{D_i}\cdot\frac{\mathrm{d}(\mathrm{z_i}\cdot\mathrm{C_i})}{\mathrm{dx}}}{\sum \mathrm{D_i}\cdot \mathrm{z_i^2}\cdot \mathrm{C_i}}\right\} = -2\cdot\left\{\frac{\sum \mathrm{D_i}\cdot\frac{\mathrm{d}(\mathrm{z_i}\cdot\mathrm{C_i})}{\mathrm{dx}}}{\sum \mathrm{D_i}\cdot \mathrm{I_i}}\right\} \quad (19)$$

The above considerations justify analysis of the $CaCO_3$ crystallization system by the simplified form of Eq. 18:

$$\mathbf{J}_\mathrm{i} = -\mathrm{D_i}\frac{\mathrm{dC_i}}{\mathrm{dx}} \quad (20)$$

Rigorous and Simplified Equations

This section presents a rigorous model describing precipitation of $CaCO_3$ from a supersaturated solution followed by simplified models based on relaxed assumptions. The rigorous model takes into account multicomponent diffusional transport of all carbonic ionic species while maintaining the equilibria of the carbonate system. The simplified models are based on an average diffusion coefficient for all ions while diffusional transport of H^+ and OH^- is neglected.

Rigorous analysis

It is well established that the ionic species involved in the second dissociation constant of carbonic acid (H^+, HCO_3^-, and CO_3^{2-}) reach an instantaneous equilibrium during the precipitation reaction. This is not the case for the first dissociation constant of carbonic acid, because one of the reactants (CO_2) is not in an ionic state. However, if the CO_2 reaction is sufficiently fast, it can be assumed that reactants involved in the first dissociation constant (H^+, HCO_3^-, and CO_2) also hold an instantaneous equilibrium. This assumption simplifies Eq. 17 into:

$$\frac{dJ_i}{dx} = 0 \quad (21)$$

The diffusional transport of the various species is then simply given by:

$$J_i = k_{D_i}(c_B - c_{\mathrm{int}}) \quad (22)$$

where C_B and C_{int} are the bulk and interfacial concentration, respectively, of species i, and k_{Dj} denotes the mass transfer coefficient of the diffusing species.

Given the bulk composition of the supersaturated solution $(Ca^{2+}, CO_3^{2-}, HCO_3^-, OH^-, H^+, CO_2)$ and the mass transfer coefficients of the various species $(k_{Ca^{2+}}, k_{CO_3^{2-}}, k_{HCO_3^-}, k_{OH^-}, k_{H^+}, k_{CO_2})$, the unknown parameters are the interfacial composition $(Ca_{int}^{+2}, CO_{3int}^{2-}, HCO_{3int}^-, OH_{int}^-, H_{int}^+, CO_{2int})$, and the fluxes of the various species $(J_{Ca^{2+}}, J_{CO_3^{2-}}, J_{HCO_3^-}, J_{OH^-}, J_{H^+}, J_{CO_2}, J_{CaCO_3})$. The 13 unknown parameters are determined by the solution of the following set of 13 equations:

Balance equations

$$J_{\mathrm{Ca^{+2}}} = J_{\mathrm{CaCO_3}} \quad (23)$$

$$2J_{\mathrm{Ca^{+2}}} = J_{\mathrm{HCO_3^-}} + 2J_{\mathrm{CO_3^{-2}}} + J_{\mathrm{OH^-}} - J_{\mathrm{H^+}} \equiv J_\mathrm{T} \quad (24)$$

$$J_{\mathrm{Ca^{+2}}} = J_{\mathrm{HCO_3^-}} + J_{\mathrm{CO_3^{-2}}} + J_{\mathrm{CO_2}} \quad (25)$$

Transport equations

$$J_{\mathrm{Ca^{+2}}} = k_{\mathrm{Ca^{+2}}}(\mathrm{Ca^{+2}} - \mathrm{Ca_{int}^{+2}}) \quad (26)$$

$$J_{\mathrm{CO_3^{2-}}} = k_{\mathrm{CO_3^{2-}}}(\mathrm{CO_3^{-2}} - \mathrm{CO_{3\,int}^{-2}}) \quad (27)$$

$$J_{\mathrm{HCO_3^-}} = k_{\mathrm{HCO_3^-}}(\mathit{HCO_3^-} - \mathrm{HCO_{3\,int}^-}) \quad (28)$$

$$J_{\mathrm{H^+}} = k_{\mathrm{H^+}}(\mathrm{H^+} - \mathrm{H_{int}^+}) \quad (29)$$

$$J_{\mathrm{OH^-}} = k_{\mathrm{OH^-}}(\mathrm{OH^-} - \mathrm{OH_{int}^-}) \quad (30)$$

$$J_{\mathrm{CO_2}} = k_{\mathrm{CO_2}}(\mathrm{CO_{2int}} - \mathrm{CO_2}) \quad (31)$$

Equilibria conditions

$$\frac{[\mathrm{H^+}][\mathrm{HCO_3^-}]}{[\mathrm{CO_2}]} = \frac{[\mathrm{H^+}]_{\mathrm{int}}[\mathrm{HCO_3^-}]_{\mathrm{int}}}{[\mathrm{CO_2}]_{\mathrm{int}}} = K_1' \quad (32)$$

$$\frac{[\mathrm{H^+}][\mathrm{CO_3^{-2}}]}{[\mathrm{HCO_3^-}]} = \frac{[\mathrm{H^+}]_{\mathrm{int}}[\mathrm{CO_3^{-2}}]_{\mathrm{int}}}{[\mathrm{HCO_3^-}]_{\mathrm{int}}} = K_2' \quad (33)$$

$$[\mathrm{H^+}][\mathrm{OH^-}] = K_w' \quad (34)$$

Surface integration reaction

$$J_{\mathrm{CaCO_3}} = k_R[(\mathrm{Ca^{+2}})_{\mathrm{int}}(\mathrm{CO_3^{-2}})_{\mathrm{int}} - K_{\mathrm{SP}}'] \quad (35)$$

Rate coefficient of the surface reaction

The rate coefficient k_R (m^4/s mol) of the surface reaction has been shown to depend on temperature according to the Arrhenius equation:

$$\ln k_R = \ln k_0 - E/\mathrm{RT} \quad (36)$$

Table 2 summarizes literature values of the frequency coefficient k_0 and the activation energy E:

Table 2. Literature Values of the Calcite Crystallization Rate Coefficient

Reference	Experimental System	Value of k_o	Activation Energy (J/mol)
[1]	Seeded growth experiments	3.43×10^7 L/mol min per mg seeds/L	45,830
[3]	Seeded growth experiments	6.56×10^7 L/mol min per mg seeds/L	42,920
[8]	Falling film	6.67×10^{16} cm/s per g $CaCO_3/cm^3$	86,250
[18]	Falling film	3.66×10^{13} cm/s per g $CaCO_3/cm^3$	72,210

Mass transfer coefficient $\mathbf{k_D}$

Mass transfer correlations under turbulent flow have the following general form:

$$Sh = \frac{k_D \cdot l}{D} = a \cdot \mathrm{Re}^b \cdot Sc^c \tag{37}$$

where Sh is the Sherwood number, k_D is the convective mass transfer coefficient, l is the flow passage diameter, D is the diffusion coefficient, Re is the Reynolds, and Sc is the Schmidt number. Several mass transfer coefficient correlations are available[19–24] showing somewhat different values of the exponents appearing in Eq. 37. The presents study is based on the most widely used correlation developed by Linton and Sherwood:

$$\frac{k_{D_i}}{U} = 0.023 \cdot Re^{-0.17} Sc^{-2/3} \tag{38}$$

It may be noted that the effect of the solution ionic strength on the mass transfer coefficient is negligible for usual water compositions in which the level of total dissolved solids is less than 0.1 M (around 6 g/L). For instance, the diffusion coefficient of an aqueous solution containing 0.1 M of NaCl at 25°C is 92% of the infinite dilution diffusion coefficient. As the k_{D_i} varies with $D_i^{0.67}$, the ionic strength will affect the mass transfer coefficient by only 5%.

Simplified models

Simplified models for high pH and low pH conditions were derived by assuming that the transport coefficients k_i are equal and neglecting the transport of H^+ and OH^- ions. The difference between the two models lies in the assumption made on the predominating carbon species, as described below. Confrontation of the simplified models with experimental data showed in general satisfactory agreement.[7–8,18,9]

Low pH simplified equation

The low pH model is based on the simplification that the CO_3^{-2} concentration is negligibly small so that the carbon species that need to be taken into account are HCO_3^- and CO_2. The transport equations and the surface reaction are then described by:

$$J_{CaCO_3} = K_D\left[\mathrm{Ca}^{+2} - \mathrm{Ca}_{\mathrm{int}}^{+2}\right] \tag{38}$$

$$= k_D\left[\frac{\mathrm{HCO}_3^-}{2} - \frac{\mathrm{HCO}_{3\ \mathrm{int}}^-}{2}\right] \tag{39}$$

$$= k_D[\mathrm{CO}_{2\mathrm{int}} - \mathrm{CO}_2] \tag{40}$$

$$= k_R\left[\left(\mathrm{Ca}_{\mathrm{i}}^{+2}\right)\left(\mathrm{CO}_{3\ \mathrm{int}}^{-2}\right) - K'_{sp}\right] \tag{41}$$

and K_D is evaluated from:

$$\frac{1}{k_D} = \left\{\frac{1}{k_{\mathrm{Ca}^{2+}}} + \frac{1}{k_{\mathrm{HCO}_3^-}} + \frac{1}{k_{\mathrm{CO}_2}}\right\}\Big/ 3 \tag{42}$$

Elimination of the unknown interfacial concentrations yields the following expression for the crystallization flux:

$$\left(\frac{J_{\mathrm{CaCO}_3}}{k_R} + K'_{sp}\right)\left(\frac{J_{\mathrm{CaCO}_3}}{k_D} + \mathrm{CO}_2\right) = \frac{4K'_2}{K'_1}\left(\mathrm{Ca}^{+2} - \frac{J_{\mathrm{CaCO}_3}}{k_D}\right)\left(\frac{\mathrm{HCO}_3^-}{2} - \frac{J_{\mathrm{CaCO}_3}}{k_D}\right)^2 \tag{43}$$

Expansion of Eq. 43 yields an explicit expression for the crystallization flux:

$$-\frac{4K'_2}{K'_1}\left(\frac{J_{\mathrm{CaCO}_3}}{k_D}\right)^3\frac{1}{\mathrm{CO}_2} + \left(\frac{J_{\mathrm{CaCO}_3}}{k_D}\right)^2\frac{Ca^{+2}}{\mathrm{CO}_2}\cdot B - \frac{J_{\mathrm{CaCO}_3}}{k_{o_L}} + \left[\left(\mathrm{Ca}^{+2}\right)\left(\mathrm{CO}_3^{-2}\right) - K'_{sp}\right] = 0 \tag{44}$$

where B and $\frac{1}{k_{o_L}}$ are given by:

$$B = \frac{4K'_2}{K'_1}\left(1 + \frac{\mathrm{HCO}_3^-}{\mathrm{Ca}}\right)\left(\frac{J_{\mathrm{CaCO}_3}}{k_D} + \mathrm{CO}_2\right) = \frac{4K'_2}{K'_1}\left(\mathrm{Ca}^{+2} - \frac{J_{\mathrm{CaCO}_3}}{k_D}\right)\left(\frac{\mathrm{HCO}_3^-}{2} - \frac{J_{\mathrm{CaCO}_3}}{k_D}\right)^2 \tag{45}$$

$$\frac{1}{k_{o_L}} = \frac{1}{k_D}\left[\left(\mathrm{CO}_3^{-2}\right) + \frac{4\left(\mathrm{Ca}^{+2}\right)\left(\mathrm{CO}_3^{-2}\right)}{\left(\mathrm{HCO}_3^-\right)} + \frac{K'_{sp}}{\left(\mathrm{CO}_2\right)}\right] + \frac{1}{k_R} \tag{46}$$

At low fluxes, the cubic term is negligible compared with other terms. Equation 44 may be then solved and rearranged in the form of:

$$J_{\mathrm{CaCO}_3} = \frac{k_{oL}\left[\left(\mathrm{Ca}^{+2}\right)\left(\mathrm{CO}_3^{-2}\right) - K'_{sp}\right]}{G} \tag{47}$$

where G is given by

$$G = \frac{1 + \sqrt{1 - B\left[\frac{2\mathrm{Ca}^{+2}}{k_D} - \frac{1}{k_{o_L}}\right]^2 \cdot \frac{\mathrm{CO}_3^{-2}}{\mathrm{CO}_2} \cdot \left[1 - \frac{K'_{sp}}{\left(\mathrm{Ca}^{+2}\right)\left(\mathrm{CO}_3^{-2}\right)}\right]}}{2} \tag{48}$$

When the interfacial reaction resistance ($1/k_R$) of Eq. 46 is negligibly small compared with the transport term, and the

HCO_3^- is much higher than Ca concentrations, Eq. 47 reduces to:

$$J_{CaCO_3} = k_D\left(Ca^{+2}\right)\cdot\frac{\left\{\left(CO_3^{-2}\right)-\frac{K_{sp}}{Ca^{+2}}\right\}}{\left\{\left(CO_3^{-2}\right)+\frac{K_{sp}}{Ca^{+2}}\right\}}\approx k_D\left(Ca^{+2}\right) \quad (49)$$

Similarly, when the Ca^{+2} concentration is much higher than the HCO_3^- concentration, Eq. 49 reduces to:

$$J_{CaCO_3} = \frac{k_D\left(HCO_3^-\right)}{2} \quad (50)$$

High-pH simplified equations

The high pH model is based on the simplification that the CO_2, and HCO_3^- concentrations are negligibly small so that the only carbon species need to be taken into account is CO_3^{2-}. The transport equations and the surface reaction are then simply described by:

$$J_{CaCO_3} = k_D\left(Ca^{+2}-Ca_{int}^{+2}\right) \quad (51)$$

$$= k_D\left(CO_3^{-2}-CO_{3\,int}^{-2}\right) \quad (52)$$

$$= k_R\left(\left(Ca_{int}^{+2}\right)\left(CO_{3int}^{-2}\right)-K'_{sp}\right) \quad (53)$$

where, by analogy to the Nernst binary diffusion equation, the average value of k_D is given by:

$$\frac{1}{k_D} = \left(\frac{1}{k_{Ca^{+2}}}+\frac{1}{k_{CO_3^{-2}}}\right)\Big/2 \quad (54)$$

Elimination of the unknown interfacial concentrations, the final result obtained can be most instructively expressed in the following form:

$$J_{CaCO_3} = \frac{K_o\left[\left(Ca^{+2}\right)\left(CO_3^{-2}\right)-K'_{sp}\right]}{F} \quad (55)$$

where the parameter F is given by

$$F = \frac{1+\sqrt{1-\left\{1-\frac{K'_{sp}}{\left(Ca^{+2}\right)\left(CO_3^{-2}\right)}\right\}\cdot\left\{\frac{\left(Ca^{+2}+CO_3^{-2}\right)}{k_D}\Big/\frac{1}{K_o}\right\}^2\cdot\left\{\frac{2}{\sqrt{\frac{Ca^{+2}}{CO_3^{-2}}}+\sqrt{\frac{CO_3^{-2}}{Ca^{+2}}}}\right\}^2}}{2} \quad (56)$$

and K_o, the overall crystallization coefficient, is given by:

$$\frac{1}{K_o} = \frac{\left[\left(Ca^{+2}\right)+\left(CO_3^{-2}\right)\right]}{k_D}+\frac{1}{k_R} \quad (57)$$

Equation 57 shows that the overall resistance to crystallization is governed by two resistances in series—a resistance due to diffusional transport followed by a resistance due to the interfacial crystallization process. When the interfacial reaction resistance ($1/k_R$) of Eq. 57 is negligibly small compared with the transport term and the Ca^{+2} and the CO_3^{-2} concentrations do not differ much, Eq. 55 reduces to:

$$J_{CaCO_3} = k_D\left[\sqrt{\left(Ca^{+2}\right)\left(CO_3^{-2}\right)}-\sqrt{K'_{sp}}\right] \quad (58)$$

Comparison of Results of Rigorous and Simplified Models

Simulations were carried out to compare results of the various models so as to establish the range of conditions under which the simplified equations may be used. The criterion selected for considering that the simplified equation provides a good approximation was that the absolute deviation from the accurate result is less than 10%. Table 3 summarizes values of parameters used in the simulations.

Effect of the pH level on the precipitation rate

Figures 2–4 illustrate the general effect of the pH level on the precipitation rate evaluated at various concentrations and Reynolds numbers by both the rigorous model and the simplified equations. The data plotted in Figures 2 and 3 show precipitation rates obtained at $Re = 11{,}100$ and calcium concentrations of 100 and 400 ppm, respectively, at a total alkalinity (TA) of 500 ppm as $CaCO_3$. Agreement between the rigorous and simplified equations is obtained at both Ca concentrations when the pH is less than 7.5–7.8, for the low pH equation and above 9.2–9.5, for the high pH equation.

The typical effect of increasing the Reynolds number to 22,200 is displayed in the results plotted in Figure 4, for Ca

Table 3. Physicochemical Parameters Used in the Simulations

Total Alkalinity (100–500 ppm as $CaCO_3$)		Calcium (100–400 ppm)	
Re = 4400–22,200			
K_1	$4.39\cdot\times 10^{-4}$ (mol/m^3)	D_H	$9.31\cdot\times 10^{-9}$ (m^2/s)
K_2	$4.67\cdot\times 10^{-8}$ (mol/m^3)	D_{OH}	$5.27\cdot\times 10^{-9}$ (m^2/s)
K_w	$1.88\cdot\times 10^{-8}$ (mol^2/m^6)	D_{CO2}	$2.00\cdot\times 10^{-9}$ (m^2/s)
K_R	$3.68\cdot\times 10^{-5}$ (m^4/(mol s))	D_{HCO3}	$1.13\cdot\times 10^{-9}$ (m^2/s)
K_{sp}	$3.32\cdot\times 10^{-3}$ (mol^2/m^6)	D_{CO3}	$0.97\cdot\times 10^{-9}$ (m^2/s)
K_{CO2}	$3.14\cdot\times 10^{-5}$–$1.98\cdot\times 10^{-4}$ (m/s)	D_{Ca}	$0.79\cdot\times 10^{-9}$ (m^2/s)
pH	7–11	Temp.	25 (°C)
U	24.25–198 (m/s)	l	0.025–0.05 (m)

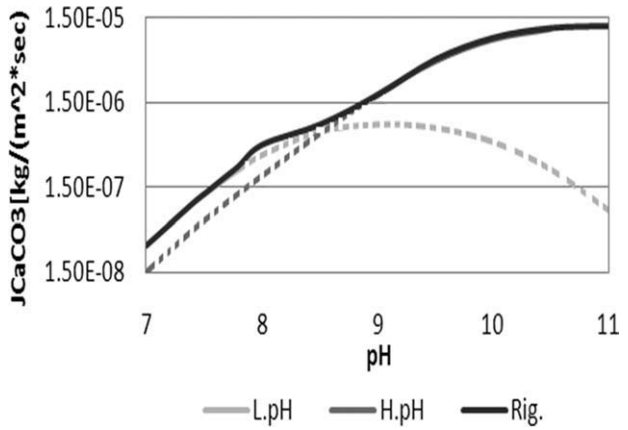

Figure 2. Precipitation flux as a function of pH (*Re* = 11,000, Ca^{2+} = 100 ppm, and TA = 500 ppm as $CaCO_3$).

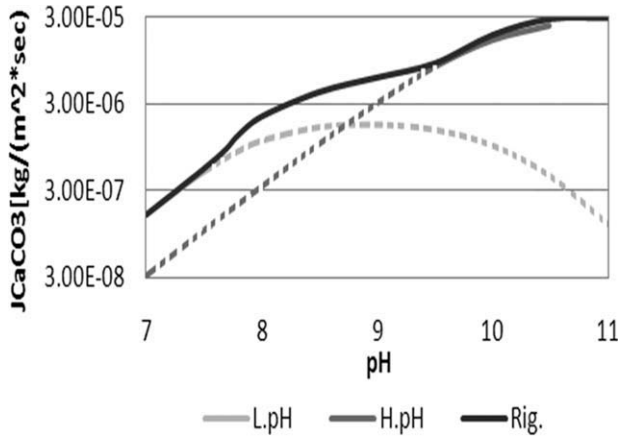

Figure 3. Precipitation flux as a function of pH (*Re* = 11,000, Ca^{2+} = 400 ppm, and TA = 500 ppm as $CaCO_3$).

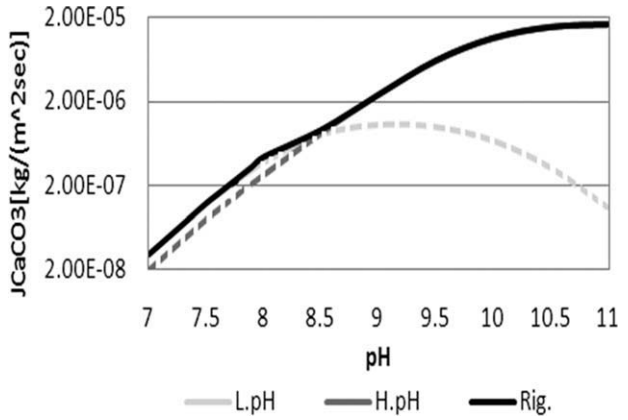

Figure 4. Precipitation flux as a function of pH (*Re* = 22,200, Ca^{2+} = 100 ppm, TA = 500 ppm as $CaCO_3$).

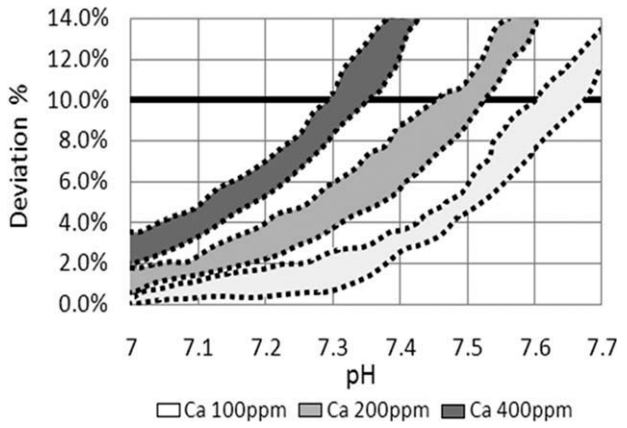

Figure 5. Absolute deviations of the low pH model at *Re* = 4400 and TA = 100–500 ppm as $CaCO_3$.

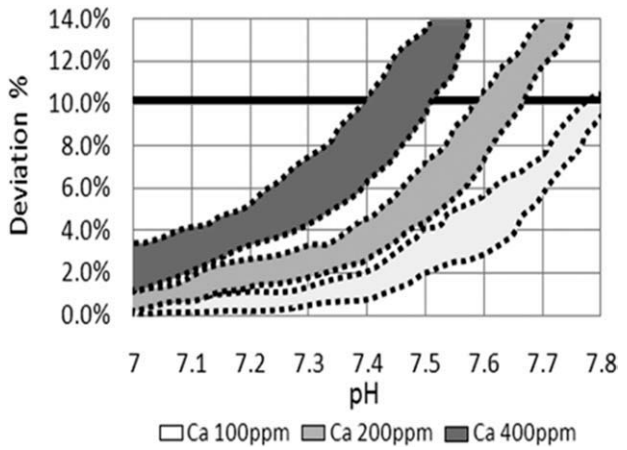

Figure 6. Absolute deviations of the low pH model at *Re* = 11,100 and TA = 100 to 500 ppm as $CaCO_3$.

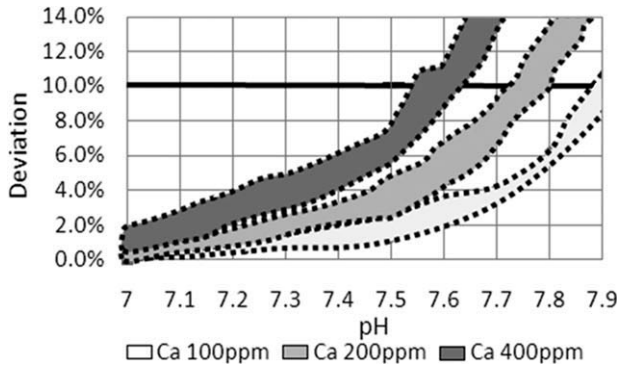

Figure 7. Absolute deviations of the low pH model at *Re* = 22,200 and TA = 100–500 ppm as $CaCO_3$.

Table 4. Limiting Low pH Levels for Deviations Below 10% from the Rigorous Results

Reynolds Number	Limiting pH Levels at Ca = 100 ppm	Limiting pH Levels at Ca = 200 ppm	Limiting pH Levels at Ca = 400 ppm
4,400	7.60–7.65	7.45–7.55	7.30–7.35
11,100	7.75–7.80	7.60–7.65	7.40–7.50
22,200	7.85–7.90	7.70–7.80	7.55–7.60

= 100 ppm, at TA = 500 PPM as $CaCO_3$. The limiting pH values bounding agreement between the rigorous and simplified equations are seen to be closely similar to those obtained at *Re* = 11,000, namely pH of less than about 7.6–7.9 for the low pH equation and above 9.2–9.5 for the high pH equation.

The above examples illustrate the general result obtained by extensive calculations. The limiting pH values bounding agreement between the rigorous and simplified equations are primarily dictated by the pH level with only minor effects generated by solution concentration and Reynolds number.

Applicability limits of the low-pH simplified model

Absolute deviations in the $CaCO_3$ precipitation rate calculated by the simplified low pH model and the rigorous model are displayed in Figures 5–7 at pH levels in the range of 7.0 to 7.9, *Re* numbers in the range of 4,400–22,000, calcium concentrations in the range of 100–500 and total alkalinities in the range of 100–500 ppm as $CaCO_3$. It is seen that the applicability of the simplified low pH model is best at the lowest Ca concentration and the highest *Re* number.

Table 4 summarizes the limiting pH levels at which the $CaCO_3$ precipitation rate evaluated by the simplified low pH model deviates by less than 10% from results calculated by the rigorous model. The lowest limiting pH level of 7.3 is obtained at *Re* = 4,400 and Ca = 400 ppm. The highest limiting pH level of 7.9 is obtained at *Re* = 22,200 and Ca = 100 ppm.

Applicability limits of the high-pH simplified model

Absolute deviations in the $CaCO_3$ precipitation rate evaluated by the simplified high pH model and the rigorous model are displayed in Figures 8–10 at pH levels in the range of 9.0–11, *Re* numbers in the range of 4,400–22,000, calcium concentrations in the range of 100–400, and total alkalinities in the range of 200–500 ppm as $CaCO_3$. The trends observed in Figures 8–10 illustrate typical limiting conditions at which the high-pH simplified model provides reasonably accurate results.

Table 5 summarizes the limiting pH levels at which the $CaCO_3$ precipitation rate evaluated by the simplified high pH model deviates by less than 10% from results calculated by the rigorous model. It is seen that as in the case of the low pH model, the applicability of the high pH model is best at low Ca concentrations and high *Re* numbers. At Ca = 100 ppm and *Re* = 22,200, the high pH model can be applied over a wide pH range extending from 8.9 to 11. At Ca = 400 ppm and *Re* = 4,400, the high pH model can be applied over a narrow a pH range extending from 9.5–9.8. However,

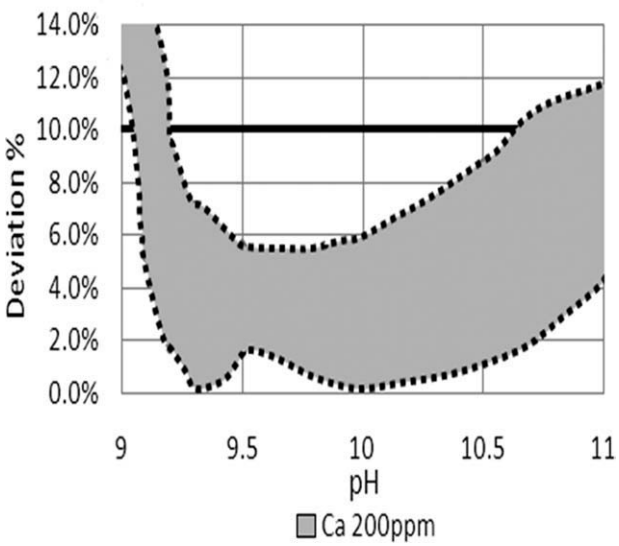

Figure 9. Absolute deviations of the high pH model at *Re* = 11,100, Ca =200 ppm, *TA* = 200-500 ppm as $CaCO_3$.

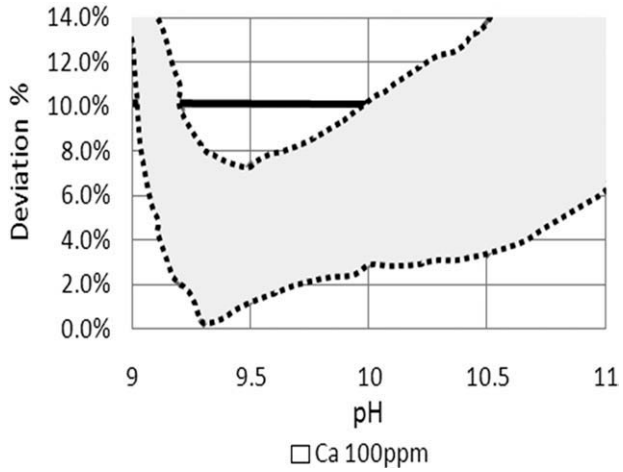

Figure 8. Absolute deviations of the high pH model at *Re* = 4,400, Ca = 100 ppm, TA = 200–500 ppm as $CaCO_3$.

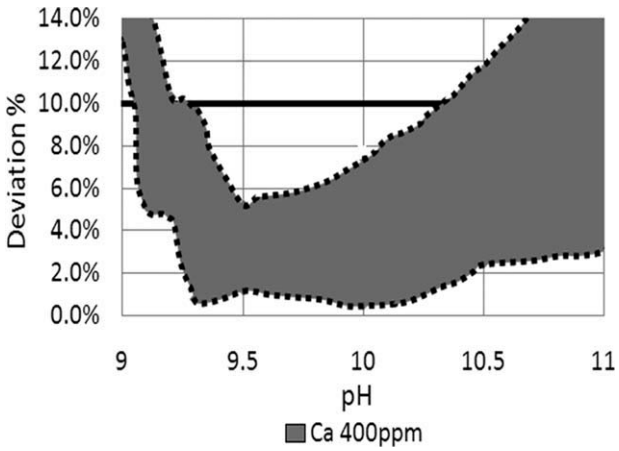

Figure 10. Absolute deviations of the high pH model deviations at *Re* = 22,200, Ca = 400 ppm, and TA = 200–500 ppm as $CaCO_3$.

Table 5. Limiting High pH Levels for Deviations Below 10% from the Rigorous Results

Reynolds Number	Limiting pH Levels at Ca = 100 ppm	Limiting pH Levels at Ca = 200 ppm	Limiting pH Levels at Ca = 400 ppm
4,400	9.2–10.0	9.45–10.0	9.5–9.8
11,100	9.1–10.6	9.25–10.60	9.3–10.0
22,200	8.9–11.0	9.15–10.75	9.25–10.40

the deviations at high total alkalinities are less pronounced. For instance, the deviation for a high calcium concentration of 400 ppm at a pH of 11 is less than 10% with *Re* numbers of 4400, 11,100, and 22,200 when TA = 500 ppm as $CaCO_3$.

Concluding Remarks

The present study describes the range of conditions at which the rate of $CaCO_3$ scale deposition in isothermal flow through a tube may be evaluated by simplified low and high pH equations. The results of the analyses show that the low pH model is usually applicable when the solution pH is below 7.6 and the high pH model usually holds when the solution pH is above 9.5.

One of the most widely encountered $CaCO_3$ scaling system is in the circulation of cooling tower water through heat exchanger tubes. The equations derived in this article can be readily adapted for predicting the rate of $CaCO_3$ scale deposition on a heat exchanger tube by evaluating solution properties and mass transfer coefficient at the surface temperature of the tube.

Notation

c = molar concentration, mol/m^3
C_B = bulk concentration of species, mol/m^3
C_{int} = interfacial concentration of species, mol/m^3
D = diffusivity coefficient, m^2/s
E = activation energy, J/mol
F = Faraday constant, s/A mol
J = ionic flux, mol/m^2 s
k_0 = pre-exponent coefficient, m^4/s mol
k_D = mass transfer coefficient, m/s
K_R = reaction constant, m^4/s mol
K_{sp} = solubility product constant, mol^2/m^6
l = flow passage diameter, m
r = rate of production
R = universal gas constant, J/mol K
Re = Reynolds number
Sc = Schmidt number
Sh = Sherwood number
T = temperature, K
u = mobility of species, s mol/kg
U = fluid velocity, m/s
V = electrical potential generated by ions motion, V
z = charge number

Subscripts

i = ionic species

Literature Cited

1. Reddy MM, Nancollas, GH. Crystallization of calcium carbonate. I. Isotopic exchange and kinetics. *J Colloid Interface Sci*. 1971;36:166–172.
2. Roques H, Girou A. Kinetic of the formation conditions of carbonate tartars. *Water Res*. 1974;8:907–920.
3. Wiechers HNS, Sturrock P, Marais GVR. Calcium carbonate crystallization kinetics. *Water Res*. 1975;9:835–845.
4. Dawe AR, Zhang Y. Kinetics of calcium carbonate scaling using observations from glass micromodels. *J Petrol Sci Eng*. 1997;18:179–187.
5. Zhang Y, Shaw H, Farquhar R, Dawe AR. The kinetics of carbonate scaling—application for the prediction of downhole carbonate scaling. *J Petrol Sci Eng*. 2001;29:85–95.
6. Paakonen TM, Riihimaki M, Puhakka E, Muurinen E, Simonson CJ, Keiski RL. Crystallization fouling of $CaCO_3$—Effect of bulk precipitation on mass deposition on the heat transfer surface. In: Proceeding of International Conference on Heat Exchanger Fouling and Cleaning VIII. Schladming, Austria, 2009:209–216.
7. Hasson D, Avriel M, Resnick W, Rozenman T, Windreich S. Mechanism of $CaCO_3$ scale deposition on heat-transfer surfaces. *Ind Eng Chem Fundamentals*. 1986;7:59–65.
8. Hasson D, Sherman H, Biton M. Prediction of calcium carbonate scaling rates. In: Proceedings of the 6th International Symposium Fresh Water from the Sea. Las Palmas, Spain, 1978;2:193–199.
9. Andritsos N, Kontopoulou M, Karabelas AJ, Koutsoukos PG. Calcium carbonate deposit formation under isothermal conditions. *Canadian J Chem Eng*. 1996;74:11–919.
10. Turner CW, Smith DW. Calcium carbonate scaling kinetics determined from radiotracer experiments with calcium-47. *Ind Eng Chem Res*. 1998;37:439–448.
11. Khan SM, Budair MO, Zubair SM. A parametric study of CaCO3 scaling in AISI 316 stainless steel tube. *Heat Mass Transf*. 2001;38:115–121.
12. Chen T, Neville A, Mingdong Y. Assessing the effect of Mg2+ on $CaCO_3$ scale formation–bulk precipitation and surface deposition. *J Cryst Growth*. 2005;275:1341–1347.
13. Chen T, Neville A, Mingdong Y. Influence of Mg2+ on CaCO3 formation—bulk precipitation and surface deposition. *Chem Eng Sci*. 2006;61:5318–5327.
14. Quan Z, Chen Y, Ma C. Heat mass transfer model of fouling process of calcium carbonate on heat transfer surface. *Sci China Ser E-Technol Sci*. 2008;51:882–889.
15. Koutsoukos PG. *Calcium carbonate scale control in industrial water systems*. In: Amjad Z, editor. *The Science and Technology of Industrial Water System*. Boca Raton, FL: CRC Press; 2010:39–60.
16. Muller-Steinhagen HM, Branch CA. Influence of thermal boundary conditions on calcium carbonate fouling in double pipe heat exchangers. *Chem Eng Process*. 1988;24:65–73.
17. Robinson RA, Stokes RH. *Electrolyte Solutions*, 2nd ed. London, UK: Butterworths; 1959.
18. Hasson D, Perl I. Scale deposition in a laminar falling film system. *Desalination*. 1981;37:279–292.
19. Linton WH, Sherwood TK. Mass transfer from solid shapes to water in streamline and turbulent flow. *Chem Eng Prog*. 1950; 46:258–264.
20. Meyerink ESC, Friedlander SK. Diffusion and diffusion controlled reactions in fully developed turbulent pipe flow. *Chem Eng Sci*. 1962;17:121–135.
21. Harriott P, Hamilton RM. Solid-Liquid mass transfer in turbulent pipe flow. *Chem Eng Sci*. 1965;20:1073–1078.
22. Shaw DA, Hanratty TJ. Turbulent mass transfer rates to a wall for large Schmidt numbers. *AIChE J*. 1977;23:28–37.
23. Berger FP, Hau KFFL. Mass transfer in turbulent pipe flow measured by the electrochemical method. *Int J Heat Mass Transf*. 1977;20:1185–1194.
24. Campbell JA, Hanratty TJ. Mechanism of turbulent mass transfer at a solid boundary. *AIChE J*. 1983;29:221–229.

Manuscript received Dec. 7, 2010, and revision received Feb. 16, 2011.